Analysis of land-based CSEM data for CO_2 monitoring at Bell Creek, MT

W. Anderson McAliley[*†], *Benjamin R. Bloss*[§], *Trevor Irons*[‡], *Nathan Moodie*[‡], *Richard Krahenbuhl*[†], *and Yaoguo Li*[†]
†*Center for Gravity, Electrical, and Magnetic Studies, Department of Geophysics, Colorado School of Mines*
§*Geology, Geophysics, and Geochemistry Science Center, United States Geologic Survey*
‡*Energy & Geoscience Institute, Civil & Environmental Engineering, University of Utah*

SUMMARY

Monitoring subsurface fluid migration is critical to any CO_2 injection operation like enhanced oil recovery or carbon storage. The controlled-source electromagnetic (CSEM) method provides a promising low-cost, non-invasive alternative to conventional monitoring methods. To investigate the use of CSEM for monitoring CO_2 injection, we are conducting a time-lapse charged well casing CSEM survey at the Bell Creek oil field. There, CO_2 is injected into the reservoir for enhanced oil recovery, which also results in incidental carbon storage. From October 2017 to October 2018 we completed three field campaigns, and we plan to complete one more in July 2019. We have analyzed the signal strength and variance of the time-lapse CSEM data. Difference data signal strength well exceeds the standard deviation of the data, and it agrees with estimates of expected signal strength derived from numerical modeling. This analysis indicates that our survey can detect the change in conductivity within the reservoir due to fluid movement.

INTRODUCTION

The Bell Creek oil field lies in southeastern Montana within the Powder River Basin (Figure 1a). The Muddy Sandstone formation holds the oil-bearing reservoir at 1400 m depth. A stratigraphic column for the region can be found in Figure 2. At that depth, the temperature and pressure are high enough to maintain CO_2 in a supercritical state, making the field amenable to CO_2 enhanced oil recovery (EOR). The overlying formations dominantly consist of shale, with some sandstone and interbedded limestone (Hamling et al., 2013).

Oil production in the area commenced in 1968. The reservoir has undergone both primary oil production and secondary water flood production. In 2013, Denbury Resources began CO_2 injection for EOR and incidental CO_2 storage. Injection began in the southern part of the field, and is moving northward in phases (Figure 1b). We focus on monitoring CO_2 injection in the phase 5 area.

Here we describe an ongoing time-lapse charged well casing controlled-source electromagnetic (CWC-CSEM) survey to monitor CO_2 migration in the subsurface. The survey is part of a collaborative project between the Colorado School of Mines, the University of Utah, the United States Geologic Survey, and the New Mexico Institute of Mining and Technology. The CWC-CSEM survey is sensitive to electrical conductivity changes in the subsurface. As CO_2 displaces electrically conductive fluids in the pore spaces of the reservoir, the bulk conductivity of the rock decreases. Thus, an electromagnetic survey can be used to monitor CO_2 movement. However, the

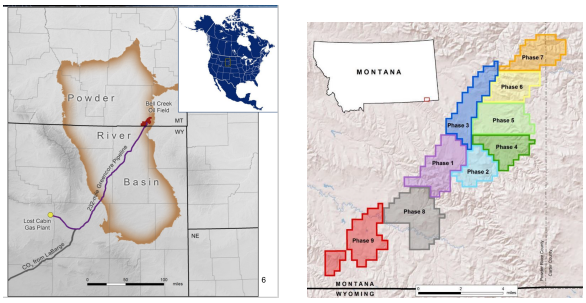

(a) (b)

Figure 1: (a) Map showing the location of the Bell Creek oil field, and the source of the CO_2 being injected, from Gorecki et al. (2014). (b) Planned CO_2 EOR production phases, from Gorecki (2016).

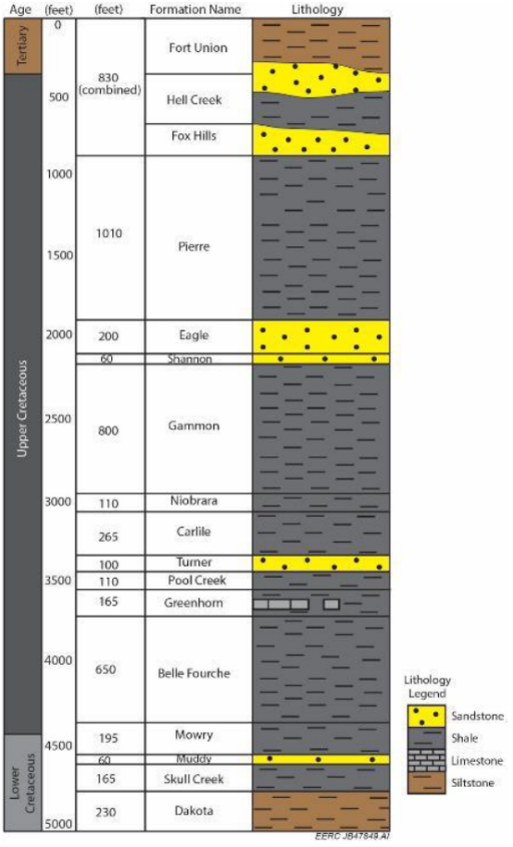

Figure 2: Stratigraphic column of the Bell Creek Area, from Gorecki et al. (2014).

conductive shale that overlies the reservoir reduces the amount of current that reaches the depth of the reservoir, weakening the time-lapse signal that arises from CO_2 movement. Therefore, imaging changes in conductivity within the reservoir is challenging. By using well casings that extend down to the reservoir depth as transmitter electrodes, more electric current can reach the reservoir and thereby increase the sensitivity of the survey to conductivity changes within the reservoir.

CWC-CSEM SURVEY

The CSEM field campaigns were carried out as follows. We connected a 30 kW Zonge GGT-30 transmitter to two well casings at a time. During the first two campaigns, we used two 12 AWG transmitter wires per casing running in parallel to minimize resistance. However, we found that we could achieve the same amount of current with a cleaner transmission signal (one that more closely resembled a square wave) using a single 10 AWG wire. Generally, well casings were used as both of the transmitter electrodes (Figure 3). Transmitter wells were spaced about 2 km apart (Figure 4a). We used three wells in any given campaign, transmitting between two wells at a time. One well pair was oriented in the northeast-southwest direction, and the other in the east-west direction. One well was shared between both pairs (Figure 4a).

We transmitted a 100% duty cycle square waveform at a range of frequencies between 0.125 Hz and 16 Hz, spaced by a factor of two. In addition, we transmitted at 0.125 Hz with a 50% duty cycle. One transmission "sweep" consisted of transmitting at least 64 periods at each frequency, from lowest to highest, followed by sixteen periods at 0.125 Hz with a 50% duty cycle. We ensured that every receiver recorded during a minimum of three sweeps per well pair. The transmitter signal was recorded at a sampling rate of 4096 Hz. Nominally, the transmitted current was 30 A, which required an output voltage of 200 V to 600 V.

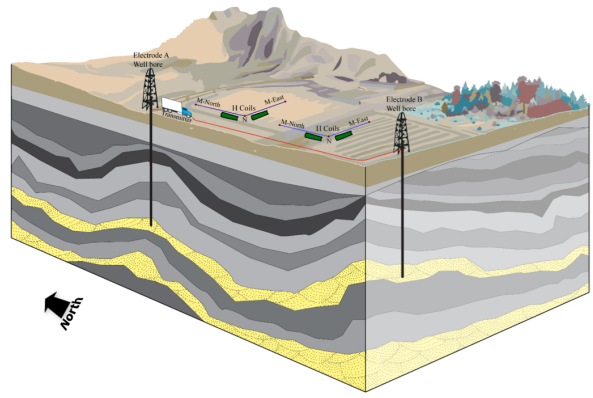

Figure 3: Schematic of the survey design showing two well casings being used as transmitter electrodes.

Receiver stations were spaced roughly 400 m apart. Zonge Zen receivers logged data at a sampling rate of 4096 Hz during active transmission. Receivers measured two horizon-

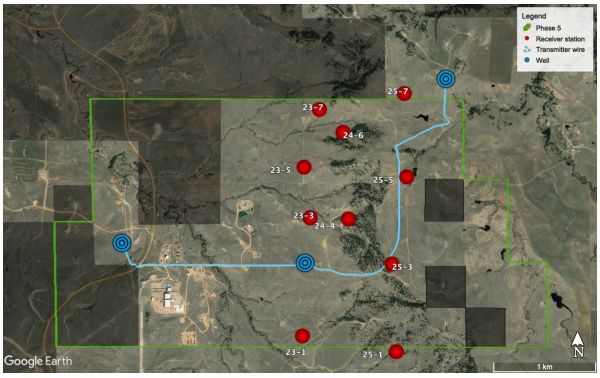

(a)

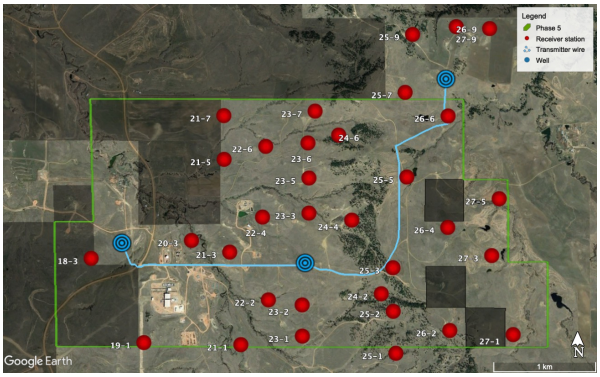

(b)

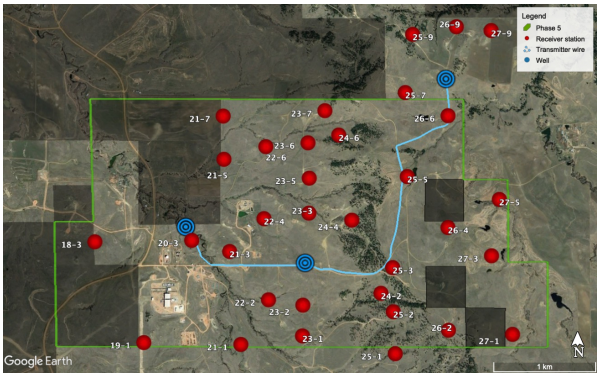

(c)

Figure 4: (a) October 2017 CSEM survey layout for (a) October 2017, (b) May 2018, and (c) October 2018 campaigns. Red dots indicate locations where the Zen receivers were. Blue dots represent the wells used as transmitter electrodes, and the blue lines represent transmitter wires. In October 2018, 10 receiver stations recorded data, while 33 stations recorded data in May and October 2018. In October 2018 the western transmitter well was inaccessible, so we were forced to transmit on a nearby well instead.

tal components of the electric field at every station. Non-polarizing Ag-AgCl electrodes were used. 100 m receiver electric dipoles were placed in an 'L' configuration, allowing orthogonal dipoles to share one electrode. The high impedance of the Zens' input channels ensured that the measurements of the two components of the electric field would remain independent, despite sharing a common electrode. Two or three spatial components of the magnetic field were also measured at most stations. Zonge Ant-4 magnetic coils were used to measure the orthogonal magnetic fields. Overnight, the receivers assumed a passive magnetotelluric recording schedule, logging data at 256 Hz with short intervals at 4096 Hz.

Figures 4a, 4b, and 4c show the survey design. Due to delays and equipment issues during the October 2017 campaign, we only recorded data at 10 receiver stations (Figure 4a). In May 2018, we expanded to 33 receiver stations (Figure 4b). We used sub-aerial dig-free installations of the magnetometers, developed by Oregon State University (Schultz et al., 2017). In October 2018, we again used sub-aerial magnetometer installations. The western well that we used in October 2017 and May 2018 was inaccessible due to renewed production, so we chose a nearby well to use for transmitting (Figure 4c).

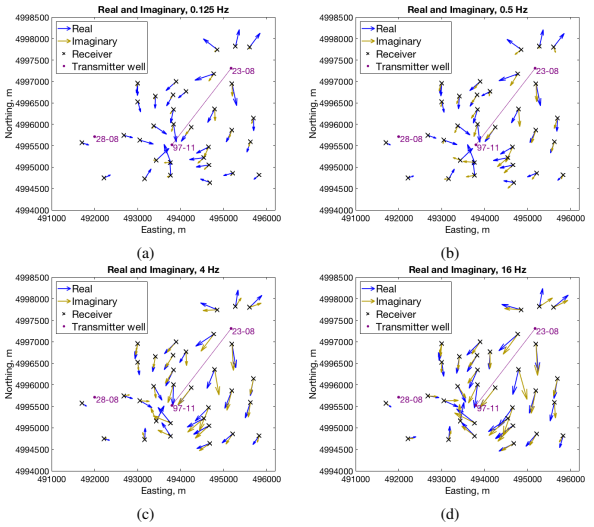

Figure 5: Real and imaginary components of the electric field transfer functions for the May 2018 campaign, transmitting between wells that are separated along the northeast-southwest direction, at (a) 0.125 Hz, (b) 0.5 Hz, (c) 4 Hz, and (d) 16 Hz. The magenta dots represent transmitter wells, and the magenta line connects the two transmitter wells used for these data.

CSEM DATA PROCESSING

The recorded time series were processed to extract the frequency-domain response. First, for each pair of receiver and transmitter signals that overlap in time, 60 Hz industrial noise was removed using a lock-in filter (Strack, 1992). The lock-in filter was applied to the portions of the signal that are 100 samples after a transmitter on-time and 40 samples before the next. Next, a drift correction was applied following Pankratov and Geraskin (2010), in which a robust running average over one source period is subtracted from the signal. Fourier coefficients were computed at odd integer multiples of the source frequency, using a boxcar window with a window length and hop length equal to the source period. Instrument calibrations were applied in the frequency domain. Then, we computed frequency-domain responses by dividing each receiver Fourier coefficient by its corresponding transmitter Fourier coefficient. We averaged the responses from one pair of receiver and transmitter signals at each frequency using the M-regression estimate, after Egbert and Booker (1986). This analysis provides frequency-dependent estimates of both the transfer function and its variance. Finally, we rotated the electric and magnetic components as needed to a consistent orthogonal coordinate system.

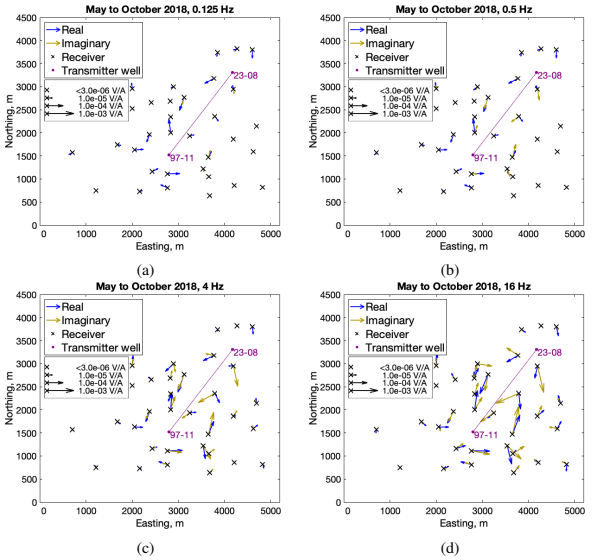

Figure 6: Time-lapse response difference between May 2018 and October 2018. Real and imaginary components of the electric field transfer functions, transmitting between wells that are separated along the northeast-southwest direction at (a) 0.125 Hz, (b) 0.5 Hz, (c) 4 Hz, and (d) 16 Hz.

SIGNAL STRENGTH

Tietze et al. (2015) analyzed the use of time-lapse borehole-to-surface CSEM for monitoring injected CO_2 at the Bockstedt oil field. They modeled the change in field strength at the surface resulting from a resistivity change from 16 Ωm to 0.6 Ωm in a three-dimensional reservoir at 1200 m depth, which is similar to the Bell Creek field. The modeling results indicate differences on the order of $10^{-9}\,\mathrm{V/(A\,m^2)}$ for

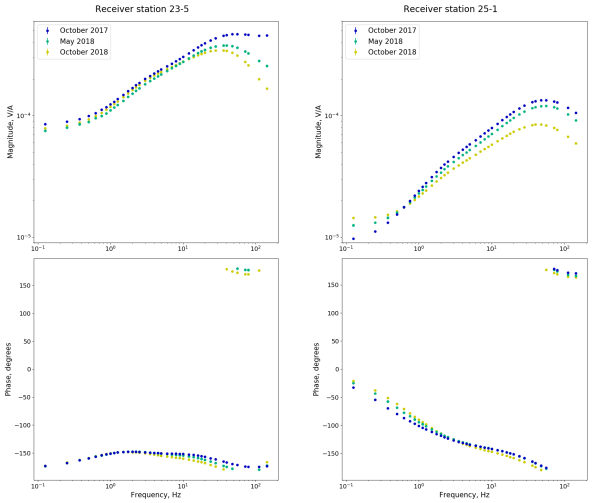

(a) (b)

Figure 7: Responses for receiver stations (a) 23-5 and (b) 25-1, for the component of the electric field in the north direction, and for transmitting between wells that are separated along the northeast-southwest direction.

the inline electric field component at low frequencies, and $10^{-12}\,\mathrm{V}/(\mathrm{A\,m}^2)$ at high frequencies. The cross-line component of the magnetic field exhibited an absolute difference upwards of $10^{-10}\,\mathrm{A}/(\mathrm{A\,m}^2)$.

At Bell Creek, our measured electric field response differences are on the order of $10^{-5}\,\mathrm{V/A}$ at low frequencies (Figures 7a and 7b. After accounting for receiver and transmitter dipole lengths, this corresponds to differences on the order of $10^{-10}\,\mathrm{V}/(\mathrm{A\,m}^2)$. At high frequencies, differences are on the same order of magnitude or larger. The large differences at high frequencies are likely due in part to changes in receiver location or transmitter wire path. Since the locations of receivers and transmitter wire path are recorded during each campaign, the effects on the time-lapse signal can be mitigated.

The magnetic field response difference at the lowest frequency is on the order of $10^{-5}\,\mu\mathrm{T/A}$. These values correspond to differences on the order of $10^{-9}\,\mathrm{A}/(\mathrm{A\,m}^2)$ after accounting for the transmitter dipole length. Like the electric field data, high frequency magnetic response differences are equally large or larger.

Standard deviations are estimated based on response functions computed from different time windows of the signal. Estimated standard deviations of the magnitude of the response functions are less than one percent of the magnitude, which are significantly below the magnitude of the time-lapse differences.

CONCLUSIONS

We find that the measured time-lapse CSEM signal well exceeds the estimated standard deviation of the measurements. Additionally, the magnitude of the time-lapse response difference agrees with the expected magnitude as published by Tietze et al. (2015), for both the electric and magnetic fields. These differences are significantly larger than the variance in the data, and the differences are coherent across multiple frequencies. Some part of the differences are due to small changes in survey geometry, which can be taken into consideration during modeling and inversion. The sign of the differences is consistent among multiple receiver stations, which also suggests that a time-lapse signal arising from CO_2 movement is detected by the survey.

FUTURE WORK

The final field campaign will occur in July 2019. Upon completion, the CSEM data can be analyzed and interpreted for CO_2 movement. First, the electromagnetic response to conductivity models built from the reservoir model and induction logs will be modeled. To construct the conductivity model, we use Archie's Law to link host rock type and fluid saturation to in-situ conductivity. This modeling will be done for different history-matched reservoir simulations, allowing the measurable time-lapse EM response to CO_2 injection to be predicted.

Secondly, the CSEM data will be inverted for conductivity changes at the depth of the reservoir. The overburden conductivity model may be improved by inverting all CSEM campaign data at once. Inversions of overnight MT data from the CSEM receiver stations may inform the overburden conductivity model. Once a model of the conductivity of the overburden has been established, the time-lapse CSEM data can be inverted for conductivity changes within the reservoir. These changes will be interpreted to estimate CO_2 movement.

ACKNOWLEDGMENTS

The authors would like to express their sincere thanks to Denbury Resources for their cooperation and assistance. We also gratefully acknowledge the collaborative partnership of the University of North Dakota Energy & Environmental Research Center (EERC). We thank Kylee Underwood at the Department of Energy for her support of this project. We are grateful to the members of our field crew for their invaluable assistance: Max Pace, Katrina Zamudio, Joseph Capriotti, Arvind Parapuza, Carlos Macedo, Xiaoyu Zhu, and Zachary Zyla. This research is supported by the National Energy Technology Laboratory at the Department of Energy through DOE/NETL award number FE-0028320. The work is also supported in part by a scholarship from the Society of Exploration Geophysicists.

REFERENCES

Egbert, G. D., and J. R. Booker, 1986, Robust estimation of geomagnetic transfer functions: Geophysical Journal International, **87**, 173–194.

Gorecki, C. D., 2016, Plains CO2 reduction (PCOR) partnership: Bell Creek field project: 2016 mastering the subsurface through technology innovation and collaboration: Carbon storage and oil and natural gas technologies review meeting.

Gorecki, C. D., E. Steadman, and J. Harju, 2014, Plains CO2 reduction (PCOR) partnership - phase III: 2014 carbon storage R&D project review meeting.

Hamling, J., C. Gorecki, R. Klapperich, D. Saini, and E. Steadman, 2013, Overview of the Bell Creek combined CO2 storage and CO2 enhanced oil recovery project: Energy Procedia, **37**, 6402 – 6411. (GHGT-11 Proceedings of the 11th international conference on greenhouse gas control technologies, 18-22 November 2012, Kyoto, Japan).

Pankratov, O. V., and A. I. Geraskin, 2010, On processing of controlled source electromagnetic (CSEM) data: Geologica acta, **8**, 31–49.

Schultz, A., N. L. Bennington, E. Bowles-martinez, N. Imamura, R. A. Cronin, D. J. Miller, L. Hart, R. M. Gurrola, B. A. Neal, K. Scholz, B. Fry, and R. Carbonari, 2017, Controls on magmatic and hydrothermal processes at Yellowstone supervolcano: The wideband magnetotelluric component of an integrated MT/seismic investigation: AGU Fall Meeting Abstracts.

Strack, K.-M., 1992, Exploration with deep transient electromagnetics: Elsevier Amsterdam.

Tietze, K., O. Ritter, and P. Veeken, 2015, Controlled-source electromagnetic monitoring of reservoir oil saturation using a novel borehole-to-surface configuration: Geophysical Prospecting, **63**, 1468–1490.